

high-work-function contact. For the same reason, electrons are extracted from C_{60} at the Ca/MEH-PPV: C_{60} interface. The result, then, is that separated carriers are not "wasted"; they are automatically collected by the proper electrode so that external work can be done.

The substantial enhancement in η_c achieved with the bicontinuous D-A network material results from the large increase in the interfacial area over that in a D-A bilayer and from the relatively short distance from any point in the polymer to a charge-separating interface. Moreover, the internal D-A junctions inhibit carrier recombination and thereby improve the lifetime of the photoinduced carriers (6), so that the separated charge carriers can be efficiently collected by the built-in field from the asymmetric electrodes. Similar effects have been observed in MEH-PPV: Cyano-PPV polymer blends (10, 11).

The device efficiencies are not yet optimized. Because only ~60% of the incident power was absorbed at 430 nm in the thin-film devices used for obtaining the data in Fig. 3, the internal carrier collection efficiency and energy conversion efficiency are approximately 1.7 times larger; that is, $\eta_c \approx 90\%$ e/ph and $\eta_e \approx 5.5\%$ at $10 \mu\text{W}/\text{cm}^2$. Although nearly 100% absorption can be achieved by using thicker films, η_c is currently limited in thick-film devices by internal resistive losses. Further improvements in device efficiencies are expected when the blend composition and the network morphology are optimized.

REFERENCES AND NOTES

- For a review of photovoltaic devices made with polyacetylene, see J. Kanicki, in *Handbook of Conducting Polymers*, T. A. Skotheim, Ed. (Dekker, New York, 1986), pp. 543–660; S. Glenis, G. Tourillon, F. Garnier, *Thin Solid Films* **111**, 93 (1984); S. Karg, W. Riess, V. Dyakonov, M. Schwoerer, *Synth. Metals* **54**, 427 (1993); H. Antoniadis, B. R. Hsieh, M. A. Abkowitz, S. A. Jenekhe, M. Stolka, *ibid.* **64**, 265 (1994); R. N. Marks, J. J. M. Halls, D. D. C. Bradley, R. H. Friend, A. B. Holmes, *J. Phys. Condens. Matter* **6**, 1379 (1994); G. Yu, C. Zhang, A. J. Heeger, *Appl. Phys. Lett.* **64**, 1540 (1994).
- For an early review, see G. A. Chamberlain, *Solar Cells* **8**, 47 (1983); C. W. Tang, *Appl. Phys. Lett.* **48**, 183 (1986); B. Miller *et al.*, *J. Am. Chem. Soc.* **113**, 6291 (1991); C. H. Lee, G. Yu, D. Moses, A. J. Heeger, *Appl. Phys. Lett.* **65**, 664 (1994).
- D. Adam *et al.*, *Nature* **371**, 141 (1994).
- For examples, see B. A. Gregg, M. A. Fox, A. J. Bard, *J. Phys. Chem.* **94**, 1586 (1990); C. Y. Liu, H. L. Pan, H. Tang, M. A. Fox, A. J. Bard, *ibid.* **99**, 7632 (1995).
- N. S. Sariciftci, L. Smilowitz, A. J. Heeger, F. Wudl, *Science* **258**, 1474 (1992); N. S. Sariciftci and A. J. Heeger, *Intern. J. Mod. Phys. B* **8**, 237 (1994).
- C. H. Lee *et al.*, *Phys. Rev. B* **48**, 15425 (1993).
- G. Yu, K. Pakbaz, A. J. Heeger, *Appl. Phys. Lett.* **64**, 3422 (1994).
- N. S. Sariciftci *et al.*, *ibid.* **62**, 585 (1993).
- N. S. Sariciftci and A. J. Heeger, U.S. Patent 5,331,183 (1994); U.S. Patent 5,454,880 (1995).
- G. Yu and A. J. Heeger, *J. Appl. Phys.* **78**, 4510 (1995).
- J. J. M. Halls *et al.*, *Nature* **376**, 498 (1995).
- Electrical measurements were performed with a

Keithley 236 Source-Measure Unit. The excitation source was a tungsten-halogen lamp with a band-pass filter (centered at 430 nm, with a bandwidth of 100 nm). The maximum optical power at the sample was ~20 mW/cm².

- F. Wudl, P.-M. Allemand, G. Srdanov, Z. Ni, D. McBranch, in *Materials for Nonlinear Optics: Chemical Perspectives*, S. R. Marder, J. E. Sohn, G. D. Stucky, Eds. (American Chemical Society, Washington, DC, 1991), pp. 683–686.
- J. C. Hummelen, B. W. Knight, F. Lepec, F. Wudl, *J. Org. Chem.* **60**, 532 (1995).
- I. D. Parker, *J. Appl. Phys.* **75**, 1656 (1994).
- I. H. Campbell, D. L. Smith, J. P. Ferraris, *Appl. Phys. Lett.* **66**, 3030 (1995).
- η_e was calculated from the relation $\eta_e = FF I_{sc} V_{oc} / P_{in}$ using the following definition of filling factor:

$$FF = \int_0^{V_{oc}} IdV / I_{sc} V_{oc}$$

[see (8)]. In engineering applications, another definition of FF is sometimes used: $FF = I_m V_m / I_{sc} V_{oc}$ where I_m and V_m are current and voltage for maximum power output. The FF and the η_e following this definition are approximately half of the values shown in the text.

- The authors are grateful to N. S. Sariciftci and C. H. Lee for many valuable discussions. Supported by the Department of Energy under a grant from the Advanced Energy Projects Program (DOE-FG03-93ER12138).

20 June 1995; accepted 25 October 1995

Solution-Liquid-Solid Growth of Crystalline III-V Semiconductors: An Analogy to Vapor-Liquid-Solid Growth

Timothy J. Trentler, Kathleen M. Hickman, Subhash C. Goel, Ann M. Viano, Patrick C. Gibbons, William E. Buhro*

Until now, micrometer-scale or larger crystals of the III-V semiconductors have not been grown at low temperatures for lack of suitable crystallization mechanisms for highly covalent nonmolecular solids. A solution-liquid-solid mechanism for the growth of InP, InAs, and GaAs is described that uses simple, low-temperature ($\leq 203^\circ\text{C}$), solution-phase reactions. The materials are produced as polycrystalline fibers or near-single-crystal whiskers having widths of 10 to 150 nanometers and lengths of up to several micrometers. This mechanism shows that processes analogous to vapor-liquid-solid growth can operate at low temperatures; similar synthesis routes for other covalent solids may be possible.

Crystal growth requires either (i) a reversible pathway between a fluid phase (solution, melt, or vapor) and the solid phase or (ii) high surface or bulk mobilities in the solid phase (Fig. 1) (1). These conditions allow atoms, ions, or molecules to adopt correct positions in developing crystal lattices. Ionic and molecular solids can be crystallized from solution at low temperatures ($\leq 200^\circ\text{C}$) because their constituent ions or molecules are solvated by conventional aqueous or organic solvents, and thus, condition (i) is met. In contrast, covalent nonmolecular solids such as the III-V semiconductors typically cannot be crystallized from solution at low temperatures because conventional solvents are unable to solvate atoms or cluster fragments from their solid structures, and therefore, covalent nonmolecular solids are generally insoluble. Consequently, III-V semiconductor crystals are grown at higher temperatures, typically either from the melt [condition (i), $\geq 1000^\circ\text{C}$] (2) or by organometallic chemical vapor deposition

(OMCVD) [condition (ii), $\geq 500^\circ\text{C}$] (3).

We report a method for crystallizing the III-V compounds InP, InAs, and GaAs using simple organometallic reactions conducted at low temperatures in hydrocarbon solvents. We used well-studied chemical reactions (3–5), but with two conditions that support low-temperature crystal growth: catalysis by protic reagents and the participation of metallic flux particles. Our results are consistent with a solution-liquid-solid (SLS) crystal-growth mechanism, which is analogous to the vapor-liquid-solid (VLS) mechanism discovered by Wagner and Ellis 30 years ago (6). The III-V materials are produced in unusual polycrystalline fiber and whisker morphologies (7) with small crystal dimensions. The temperatures used are to our knowledge the lowest at which III-V compounds have been crystallized and the lowest at which VLS or analogous processes have been shown to operate.

Solution-phase syntheses have produced amorphous semiconductors [GaAs (8, 9), InP (9, 10), and Cd_3P_2 (11)] and nanocrystalline semiconductors [GaAs (12), InP (13), InAs (14), CdS (15), CdSe (15, 16), and CdTe (15)] with crystallite sizes in the range of 1 to 12 nm. The nanocrystalline semiconductors were produced under cir-

T. J. Trentler, K. M. Hickman, S. C. Goel, W. E. Buhro, Department of Chemistry, Washington University, St. Louis, MO 63130–4899, USA.

A. M. Viano and P. C. Gibbons, Physics Department, Washington University, St. Louis, MO 63130–4899, USA.

*To whom correspondence should be addressed.

Fig. 1. Crystal-growth pathways: (A) growth by reversible deposition from solution, liquid, or vapor [condition (i)], and (B) growth by irreversible deposition with high solid-phase atomic mobility [condition (ii)].

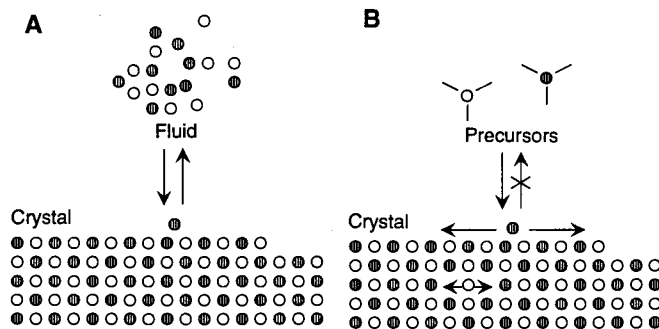
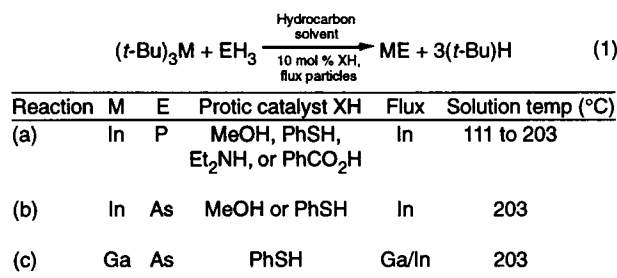


Fig. 2. The organometallic reactions. The table gives the substitutions to the general formula for reactions 1a, 1b, and 1c. Abbreviations: *t*-Bu, *tert*-butyl; Me, methyl; Ph, phenyl; and Et, ethyl.



cumstances in which conditions (i) or (ii) (Fig. 1) were apparently marginally operative. In contrast, we obtained polycrystalline fibers (20 to 50 nm by 1 μm) of InP from the solution-phase methanolysis of $\{t\text{-Bu}_2\text{In}[\mu\text{-P}(\text{SiMe}_3)_2]_2\}$ (17), which prompted our discovery of the crystal-growth mechanism described here.

The organometallic reactions (Fig. 2) were analogs to those used for depositing III-V epitaxial films by OMCVD at higher temperatures (3, 18). Previously, when such

reactions were conducted at lower temperatures in solution, alkane elimination was incomplete, leading to ill-characterized organometallic oligomers that retained large quantities of residual alkyl and E-H groups (4, 5), rather than the target III-V compounds. We now report that the use of *tri-tert*-butylindane (19) or gallane (20) precursors and catalytic amounts (10 mol %) of the protic reagents MeOH, PhSH, Et₂NH, or PhCO₂H gave the III-V compounds in yields of 50 to 100% (Fig. 2). Because the alkane content of the products and the temperatures required to achieve crystallinity were decreased in the presence of the protic reagents, we conclude that these reagents catalytically assisted alkane elimination.

Indications of a novel crystallization mechanism were observed in the synthesis of InP (reaction 1a in Fig. 2). Toluene solutions of the precursors (with 10 mol % PhSH) were stirred at room temperature (12 hours), and then the resulting yellow mixtures were heated to reflux (solution temperature, 111°C) in

a heating mantle. Black precipitates began to form within minutes, and precipitation was generally complete in ~30 min. The x-ray powder diffraction (XRD) pattern of the product (Fig. 3A) exhibited reflections for InP and metallic In only, with coherence lengths of 20 and 50 nm, respectively. Transmission electron microscopy (TEM) images revealed that the black solid consisted mainly of kinked, polycrystalline InP fibers (Fig. 4) having widths of 10 to 100 nm and lengths of up to ~1 μm. Frozen droplets (particles) of metallic In were found at the tips of many of the fibers (arrows in Fig. 4). Energy dispersive x-ray spectroscopy (EDS) confirmed the elemental composition of the InP fibers and In fiber tips. In contrast to other trialkylindanes, *t*-Bu₃In decomposes thermally or photochemically to metallic In (19); partial thermal decomposition of *t*-Bu₃In during the course of reaction 1a is the likely source of the observed In particles.

Only two growth mechanisms for crystalline fibers or whiskers are widely known: the screw-dislocation mechanism and the VLS mechanism (21). The VLS mechanism (Fig. 5A) functions at elevated temperatures under chemical-vapor-deposition conditions and promotes whisker growth of many crystalline elements and compounds (21), including silicon at 900° to 1100°C (6) and III-V semiconductors at 400° to 1000°C (22). A liquid metal or alloy droplet affixed to the whisker tip forms an interface with the growth surface; a second interface exists between the droplet and the vapor phase (Fig. 5A). Precursors in the vapor phase decompose preferentially at the vapor-liquid interface, depositing the constituent element (or elements) of the crystal phase into solution in the liquid-flux droplet. Supersaturation then supports whisker growth at the liquid-solid interface. The system selectively places the crystal face giving the lowest liquid-solid interfacial energy at the liquid-solid interface; rapid growth on this crystal facet at the interface (and the lack of growth on other facets) produces the whisker morphology. We propose a related SLS mechanism in which the precursors are delivered and react in a solution rather than in the vapor phase (Fig. 5B).

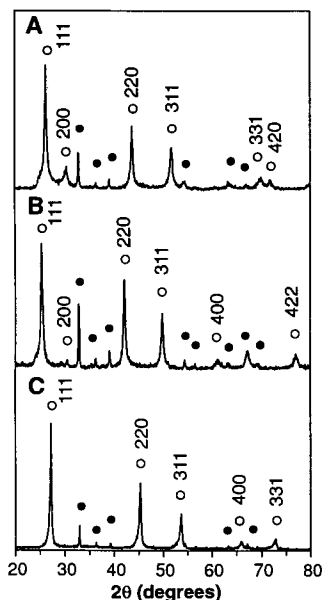


Fig. 3. The XRD patterns of the solid products from Fig. 2. (A) Reaction 1a: InP (○) and In (●); (B) reaction 1b: InAs (○) and In (●); and (C) reaction 1c: GaAs (○) and In (●).



Fig. 4. A TEM image of polycrystalline InP fibers obtained from reaction 1a (PhSH catalyst, refluxing toluene solution). The arrows point to the In flux particles (frozen droplets) at the fiber tips.

The strongest evidence for the similarity of the proposed SLS and known VLS processes was the quasi-one-dimensional growth morphologies and flux droplets attached to fiber tips in the materials. Further comparisons revealed other compelling similarities. The VLS mechanism (21) requires flux particles that are molten under the reaction conditions. The elements of the crystal phase must be soluble in the liquid (flux) phase, and at least one component should have limited solubility (to produce high supersaturations). Temperature instabilities during VLS growth introduce kinking and related irregularities into growing whiskers. Finally, whiskers of cubic compounds and elements (such as the III-V semiconductors) obtained from VLS processes typically grow along the [111] direction and exhibit crystal-

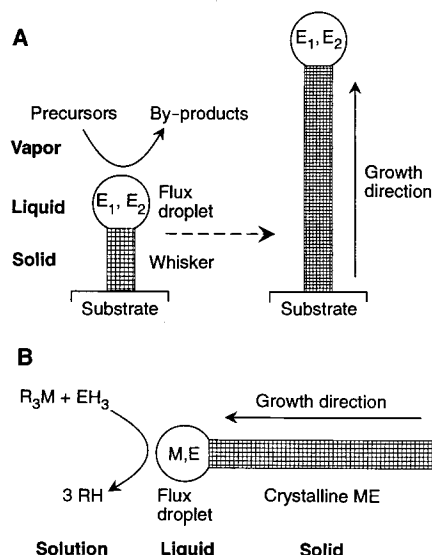


Fig. 5. Growth mechanisms. **(A)** VLS mechanism (21): the flux droplet is a metal such as Au, Ag, Pd, Pt, Ni, or Cu, and E_1 and E_2 are elements of the crystal phase dissolved in the metallic flux droplet. The whiskers on the left and right are early and late in the VLS growth process, respectively. **(B)** SLS mechanism: the flux droplet is In, and M and E are elements of the III-V semiconductor dissolved in the flux droplet. The crystalline fiber and attached flux droplet are suspended in the reaction solution.

lographically flat solid-liquid interfaces. The results below establish similar characteristics for SLS growth.

Indium metal functions as the liquid (flux) phase for the growth of InP (reaction 1a). Indium melts at 157°C, and no (low-melting) In-P eutectic has been reported (23). With oil-bath heating, bath temperatures of $\geq 157^\circ\text{C}$ were required to produce crystalline InP. With mantle heating, solution temperatures of 111°C were sufficient to produce crystalline InP because local hot spots on the reactor walls provided temperatures $\geq 157^\circ\text{C}$ for In particles collecting near them.

The In-P equilibrium phase diagram shows that P has an exceedingly low solubility in liquid In at the temperatures used in reaction 1a; the atomic fraction of P in the liquid is only $\sim 10^{-8}$ (23). A control experiment was designed to test if this level of solubility was sufficient to support InP crystallization from liquid In under our conditions. A dispersion of micrometer-sized molten In droplets (generated ultrasonically) and P_4 were allowed to react in mesitylene (1,3,5- $\text{C}_6\text{H}_3\text{Me}_3$) at 164°C. The resulting solid (after cooling) comprised micrometer-scale In spheres coated by InP crystallites, as determined by XRD and TEM analyses, confirming the ability of liquid In to serve as a crystallization flux under conditions comparable to those required in reaction 1a.

The necessity of metallic In was further established by the synthesis of crystalline InAs (reaction 1b, 1,3-diisopropylbenzene solvent). This required addition of an extra amount of $t\text{-Bu}_3\text{In}$ (10 mol %), after the excess AsH_3 was purged from the system, to allow formation of the required In particles by thermal decomposition. The XRD pattern (Fig. 3B) and TEM images of the InAs product were similar to the corresponding data for InP (Figs. 3A and 4). The kinkiness of the InP and InAs fibers was very likely caused by a lack of precise temperature control in the heating of reaction mixtures. The similarity of the InP and InAs materials reflects their production by the same SLS mechanism.

For the preparation of GaAs (reaction 1c, 1,3-diisopropylbenzene solvent), addition of 10 mol % In powder (containing 1% Mg anticaking agent) was required to induce crystallization (Fig. 3C). The TEM images revealed two prominent morphologies: kinked fibers and larger, straighter, whisker-shaped particles (Fig. 6A). The EDS analyses established 50:50 Ga:As atomic ratios in the whiskers, 1 ± 2 atomic % In in the whiskers, and Ga:In atomic ratios of 60:40 to 80:20 in the attached flux droplets. The average GaAs lattice parameter obtained by refinement of the XRD data for the sample was $a = 0.5660 \pm 0.0010$ nm, close to the standard value for GaAs of $a = 0.5654$ nm (24), indicating <2 atomic % In in solid solution in the GaAs according to Vegard's Law (25). Similar whiskers of InP were grown from reactions between $t\text{-Bu}_3\text{In}/t\text{-Bu}_3\text{Ga}$ mixtures and PH_3 (at 203°C) (Fig. 7). Analyses by EDS established 50:50 In:P atomic ratios in the whiskers, 1 ± 2 atomic % Ga in the whiskers, and In:Ga atomic ratios of 99:1 to 90:10 in the attached flux droplets. The average InP lattice parameter obtained by refinement of XRD data was $a = 0.5878 \pm 0.0010$ nm, close to the standard value of $a = 0.5869$ nm (24), indicating <2 atomic % Ga in the InP. The whisker morphology is typical for VLS growth (21).

Large regions, especially near the growth tips, of the GaAs and InP whiskers approached single-crystal character (Figs. 6 and 7). Selected-area diffraction within some linear segments of the whiskers 320 ± 30 nm in length gave single-crystal patterns (Fig. 6B). The patterns also revealed that the whisker axis (growth direction) was [111]. The structure in the linear segments was faulted zinc blende; no regions of hexagonal (wurtzite) stacking were observed. The stacking faults were in the (111) planes perpendicular to the whisker axis and appeared either as isolated twin boundaries or in more densely packed arrangements along the whisker axis. We believe these faults are responsible for the striations perpendicular to the whisker axes that are evident in Figs. 6 and 7. Note that the droplet-whisker in-

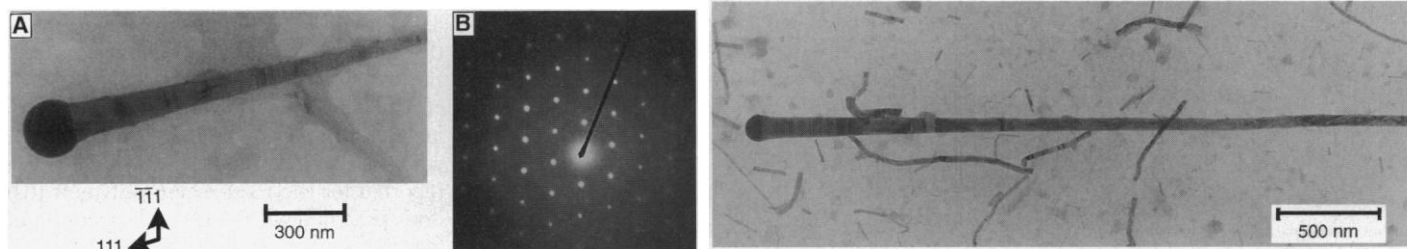


Fig. 6 (left). **(A)** TEM image of a GaAs whisker from reaction 1c (PhSH catalyst, refluxing 1,3-diisopropylbenzene solution, 203°C). The flux droplet has a Ga:In ratio of about 82:18. **(B)** Selected-area diffraction pattern from a 320 ± 30 nm single-crystal segment of the whisker in a $\langle 1\bar{1}0 \rangle$ zone establish-

ing that the whisker axis is the [111] direction. **Fig. 7 (right).** TEM image of an InP whisker from a reaction between a 50:50 $t\text{-Bu}_3\text{In}/t\text{-Bu}_3\text{Ga}$ mixture and PH_3 (PhSH catalyst, refluxing 1,3-diisopropylbenzene solution, 203°C). The flux droplet has an In:Ga ratio of about 95:5.

terfaces were flat (111) crystal faces. Thus, SLS-grown whiskers shared the crystal habit, growth direction, and interface features of VLS-grown whiskers.

Over the last several years considerable effort has been expended to develop low-temperature solution-phase molecular routes to materials, with the goals of lowering processing temperatures, producing nonthermodynamic crystal structures, and controlling crystal sizes and morphologies (17). With some exceptions (26), these endeavors have been compromised by the lack of suitable low-temperature crystallization pathways for covalent nonmolecular solids. Analogs to the high-temperature VLS crystallization method have now been found in the domain of low-temperature solution-phase chemistry, possibly opening the way to the low-temperature SLS crystallization of many other covalent solids as fibers, as whiskers, and, when sufficient control is developed, as quantum wires and quantum dots.

REFERENCES AND NOTES

1. A. W. Vere, *Crystal Growth, Principles and Progress* (Plenum, New York, 1987), chap. 1.
2. M. Dugue, J. F. Goullin, P. Merenda, M. Moulin, in *Preparative Methods in Solid State Chemistry*, P. Hagenmuller, Ed. (Academic, New York, 1972), pp. 309–360.
3. M. J. Ludowise, *J. Appl. Phys.* **58**, R31 (1985).
4. R. Didchenko, J. E. Alix, R. H. Toeniskoetter, *J. Inorg. Nucl. Chem.* **14**, 35 (1960); B. C. Harrison and E. H. Tompkins, *Inorg. Chem.* **1**, 951 (1962).
5. A. H. Cowley, P. R. Harris, R. A. Jones, C. M. Nunn, *Organometallics* **10**, 652 (1991).
6. R. S. Wagner and W. C. Ellis, *Appl. Phys. Lett.* **4**, 89 (1964).
7. "Whisker" refers to a filamentary single crystal having a large length:diameter ratio; "fiber" refers to other filamentary structures.
8. E. K. Byrne, L. Parkanyi, K. H. Theopold, *Science* **241**, 332 (1988).
9. T. Douglas, thesis, Cornell University (1991).
10. _____ and K. H. Theopold, *Inorg. Chem.* **30**, 594 (1991).
11. S. C. Goel, M. Y. Chiang, W. E. Buhro, *J. Am. Chem. Soc.* **112**, 5636 (1990).
12. M. A. Olshavsky, A. N. Goldstein, A. P. Alivisatos, *ibid.*, p. 9438; H. Uchida, C. J. Curtis, A. J. Nozik, *J. Phys. Chem.* **95**, 5382 (1991); H. Uchida, C. J. Curtis, P. V. Kamat, K. M. Jones, A. J. Nozik, *ibid.* **96**, 1156 (1992).
13. O. I. Micić, C. J. Curtis, K. M. Jones, J. R. Sprague, A. J. Nozik, *ibid.* **98**, 4966 (1994).
14. H. Uchida *et al.*, *Chem. Mater.* **5**, 716 (1993).
15. C. B. Murray, D. J. Norris, M. G. Bawendi, *J. Am. Chem. Soc.* **115**, 8706 (1993).
16. M. L. Steigerwald *et al.*, *ibid.* **110**, 3046 (1988), and references therein.
17. W. E. Buhro, *Polyhedron* **13**, 1131 (1994).
18. Phosphine and arsine are highly toxic and must be handled in accordance with proper safety measures. E. Fluck, *Fortschr. Chem. Forsch.* **35**, 1 (1973); W. Braker and A. L. Mossman, *Effects of Exposure to Toxic Gases—First Aid and Medical Treatment* (Matheson Gas Products, East Rutherford, NJ, 1970), pp. 37–38 and 86–96.
19. D. C. Bradley, D. M. Frigo, M. B. Hursthouse, B. Hussain, *Organometallics* **7**, 1112 (1988).
20. R. A. Kovar, H. Derr, D. Brandau, J. O. Callaway, *Inorg. Chem.* **14**, 2809 (1975).
21. R. S. Wagner, in *Whisker Technology*, A. P. Levitt, Ed. (Wiley, New York, 1970), chap. 3; E. I. Gilvargizov, in *Current Topics in Materials Science*, E. Kaldis, Ed. (North-Holland, Amsterdam, 1978), vol. 1, chap. 3.
22. R. L. Barns and W. C. Ellis, *J. Appl. Phys.* **36**, 2296 (1965); C. M. Wolfe, C. J. Nuese, N. Holonyak Jr., *ibid.*, p. 3790; W. C. Ellis, C. J. Frosch, R. B. Zetterstrom, *J. Cryst. Growth* **2**, 61 (1968); J. J. Nickl and W. Just, *ibid.* **11**, 11 (1971); M. Yazawa, M. Koguchi, K. Hiruma, *Appl. Phys. Lett.* **58**, 1080 (1991); M. Yazawa, M. Koguchi, A. Muto, M. Ozawa, K. Hiruma, *ibid.* **61**, 2051 (1992); M. Yazawa, M. Koguchi, A. Muto, K. Hiruma, *Adv. Mater.* **5**, 577 (1993).
23. E. Kuphal, *J. Cryst. Growth* **67**, 441 (1984).
24. A. R. West, *Solid State Chemistry and Its Applications* (Wiley, New York, 1984), p. 237.
25. _____, *ibid.*, p. 367.
26. E. Ramli, T. B. Rauchfuss, C. L. Stern, *J. Am. Chem. Soc.* **112**, 4043 (1990); S. Dev, E. Ramli, T. B. Rauchfuss, C. L. Stern, *ibid.*, p. 6385; A. F. Hepp, M. T. Andras, S. G. Bailey, S. A. Duraj, *Adv. Mater. Opt. Electron.* **1**, 99 (1992).
27. This research was funded by an NSF Presidential Young Investigator Award (CHE-9158369) to W.E.B., generously supported by Emerson Electric, Eastman Kodak, Monsanto, and Mr. and Mrs. A. H. Homeyer. K.M.H. was supported by a Department of Education Graduate Assistance in Areas of National Need grant.

29 June 1995; accepted 20 October 1995

High Photorefractive Gain in Nematic Liquid Crystals Doped with Electron Donor and Acceptor Molecules

Gary P. Wiederrecht, Beth A. Yoon, Michael R. Wasielewski

Liquid crystalline composite materials have been prepared that are strongly photorefractive. Nematic liquid crystals were doped with both electron donor and electron acceptor molecules that undergo facile, photoinduced, electron transfer reactions to yield mobile ions. A photorefractive gain ratio of 1.88 was observed. This gain ratio was achieved with low applied electric fields (0.4 kilovolts per centimeter) requiring only a 1.5-volt battery and low light intensities (100 milliwatts per square centimeter) in samples 37 to 88 micrometers thick that showed no loss in gain over a 6-month period.

Photorefractive materials hold great promise for optical device applications in the areas of reversible optical holography, noise-free optical image amplification, phase conjugate mirrors, and other optical signal processing techniques (1). The photorefractive effect is a change in the refractive index of an electrooptic material that is produced by a space-charge field resulting from photoinduced directional charge

transport over macroscopic distances within the material. A pair of coherent laser beams that are crossed in a photorefractive material produce an interference pattern that photogenerates charges in the illuminated regions. These charges migrate by diffusion, often under the influence of an applied electric field, into the dark regions of the interference pattern. The resultant space-charge field modulates the index of refraction of the material, producing a refractive index grating.

Beam coupling between the two crossed laser beams occurs by means of their interaction with the index grating, which is spatially phase-shifted relative to the optical interference pattern. The result is that

one beam gains energy at the expense of the other (2). This gain is diagnostic for the photorefractive effect in thick or volume gratings and is the basis for many of the applications listed above. A particularly exciting advance in this field came in 1991 with the discovery of photorefractivity in organic polymers (3). Subsequently, the performance of organic photorefractive materials improved very rapidly, and at present these materials have higher net photorefractive gain than do their inorganic single crystal counterparts (2, 4, 5). Such large effects have been achieved through optimization of the charge generation, charge transport, and electrooptic characteristics of the doped polymers. In addition, researchers have decreased the glass transition temperature of the polymers, which permits orientational alignment of the birefringent, nonlinear optical chromophores by a space-charge field within the viscous polymer. This nonlinear electrooptic effect, called the orientational effect, produces an additional large contribution to the total change in the index of refraction (6). In fact, the orientational effect makes a greater contribution to the photorefractive gains reported for the most recent polymers than does the traditional linear electrooptic effect (4).

On the basis of this information, nematic liquid crystals (LCs) are very attractive substances for use in photorefractive materials because they consist entirely

G. P. Wiederrecht, Chemistry Division, Argonne National Laboratory, Argonne, IL 60439–4831, USA.
B. A. Yoon, Department of Chemistry, Northwestern University, Evanston, IL 60208–3113, USA.
M. R. Wasielewski, Chemistry Division, Argonne National Laboratory, Argonne, IL 60439–4831, and Department of Chemistry, Northwestern University, Evanston, IL 60208–3113, USA.